

# A new adaptive lead-lag control scheme for high current PEM hydrogen electrolyzers

Abdelrahman M. Elhawash

*Centre for Power and Energy Systems*

INESC TEC

*Faculty of Engineering*

University of Porto

Porto, Portugal

abdelrahman.elhawash@inesctec.pt

Rui Esteves Araújo

*Centre for Power and Energy Systems*

INESC TEC

*Faculty of Engineering*

University of Porto

Porto, Portugal

raraujo@fe.up.pt

João A. Peças Lopes

*FIEEE*

*Centre for Power and Energy Systems*

INESC TEC

*Faculty of Engineering*

University of Porto

Porto, Portugal

jpl@fe.up.pt

**Abstract**—This paper aims at researching the design of a current controller for an interleaved Buck converter used to feed a high current 5 kW Polymer electrolyte membrane (PEM) electrolyzer representing a module stack level. The main challenge is to design a robust controller that ensures operation over a wide range of electrolyzer operating points while guaranteeing control requirements and current sharing between the converters. The developed control scheme ensures responsiveness to the requirements of the grid's ancillary services and control over the dynamics of the electrolyzer. MATLAB/Simulink simulation results with dSPACE compatible models are presented to validate the lead-lag controller, designed using root locus, achieving a ripple current of 0.1 A, a 0.3% steady-state error, and a settling time of 50 ms for a step response.

**Index Terms**—Lead-lag control, interleaved buck, root locus, hydrogen electrolyzer

## I. INTRODUCTION

Green Hydrogen is expected to be a main pillar in many industries and fields in the near future according to the Renewables 2022 Global Status Report [1]. This is due to their flexible operation which opens the door towards using the electrolyzers as dynamic loads that can provide grid services, and thus, facilitate their integration in the grid [2]. In particular, PEM electrolyzers are more adequate to provide these services due to their fast dynamic response [2].

However, these new operation schemes for the grid impose a new challenge for the power electronics interface between the electrolyzer and the power source (AC or DC sources). PEM electrolyzers require a high current supply, which traditionally in industry, is provided through the already matured and affordable thyristor-based converters [3]. These converters are incapable of meeting the low ripple level of the supplied high-current required by the PEM electrolyzers. This is due to the high sensitivity of the PEM electrolyzer to ripple, which affects response times "speed" of the electrolyzer and power quality requirements which are of big concern as discussed in [3]. The effect of the ripple current on the efficiency of the PEM electrolyzer is highlighted in [4], showing a major

influence on the power consumption of the electrolyzer. Since this study focuses on the connection interface of the electrolyzer with the power supply, the before-mentioned effect of the ripple current upon power consumption in [4], is of high relevance to the controller design.

To carry out these services, a system can be described as shown in Fig. 1. A PQ-controlled active rectifier would be responsible for the power quality assurance and setting the power reference point for the electrolyzer at normal and disturbance cases. This rectifier is followed by a voltage-controlled buck converter to ensure a constant DC bus voltage and to compensate for the boost nature of the active rectifier. The final stage is a current-controlled interleaved buck converter responsible for supplying a low ripple current to the electrolyzer.

Meeting this ripple requirement deems more challenging at the level of several kW scale electrolyzers, as these PEM electrolyzers require the same high current supply condition but at a lower DC voltage level [5]. Electrolyzers are constructed using stack modules that add up to the required power rating [6], [7], thus, several of these kW scale electrolyzers are to be connected together reaching the MW grid-scale hydrogen electrolyzers. Given the resistive nature of the electrolyzer at a steady state, this wide operational power range translates into a very wide load value change. Based on that, a small perturbation in cell voltage per stack causes a huge deviation in the current and, consequently, the power consumption. Therefore, by controlling the current at a low ripple level, a cleaner voltage is to be supplied ensuring high-efficiency operation [4], [9].

Several works were reported in the literature regarding the topologies and architectures that can be used for high-power hydrogen electrolyzers operation and control [10]–[13], mainly focusing on the power circuit design, linear PI controllers operating at several modes, and similarities that can be used from other industries. Linear PI controllers used to control the system around an operating point are non-sufficient for controlling the load at cases of large changes, which is the case for the PEM electrolyzer [9]. These load changes can happen very commonly if the electrolyzers are used to provide

The research leading to this work has been carried out as part of the European Union's Horizon 2020 research and innovation program under grant agreement No 101036908 (GreenH2Atlantic).

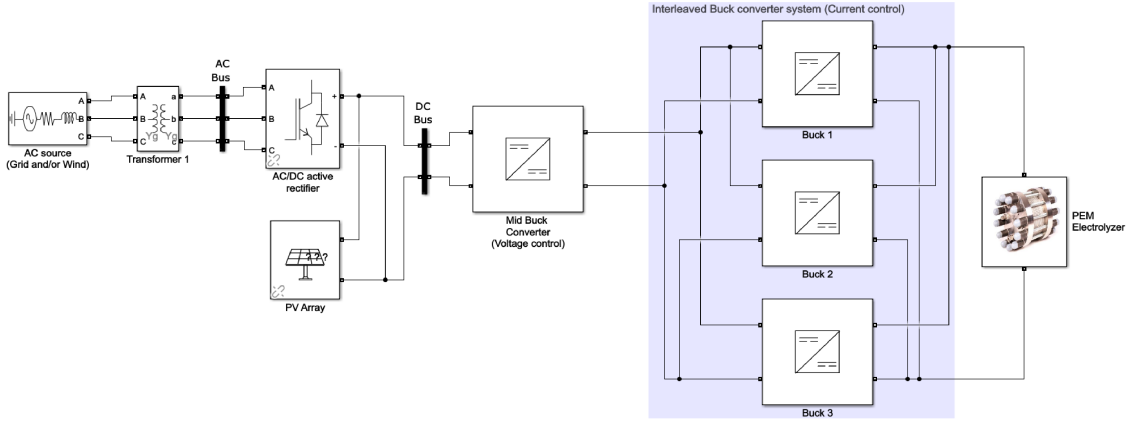


Fig. 1. Overall system overview for grid-connected PEM electrolyzer.

grid services, which come in commands for power changes following a ramp signal in the range of a few seconds in case of Frequency Containment Reserve (FCR) [8].

However, these control approaches would violate the ripple requirements of operation when applied to kW scale electrolyzer stacks operating at low voltage-high current along the full range, and add up extra complexity for the design process. For filling this gap, this paper proposes a new, simpler controller designed using root locus. The controller has the form of a lead-lag compensator that has adaptive gain and parameters depending on the operating point of the electrolyzer. This compensator places new poles and zeros in the system that assure the cancellation of the load dependency behavior, and introduces the same intended response at any given operating point while ensuring current sharing within the interleaved converter. The ease of the implementability of the controller was achieved via designing the model to be compatible with dSPACE platform for a power hardware in the loop setup that would include the interleaved converter, the hydrogen electrolyzer, a power amplifier, and a real-time digital simulator (RTDS) for the grid simulation. A 5 kW PEM electrolyzer that operates within a current range of (7.5-150) A at a voltage that ranges from (22.538-31.1) V is to be used to model a stack level for laboratory studies.

## II. METHODOLOGY AND DESIGN

The system was designed and modeled using MATLAB/Simulink software. Fig. 2 shows the developed system model. The process of designing the controller suitable for the electrolyzer under investigation starts with defining the requirements of the system, the transfer function of the current-controlled buck converter, and the design process of the suitable control scheme. The following subsections describe the development process of the investigated research.

### A. Power circuit and electrolyzer model

The electrolyzer mentioned in section (I) has the V-I steady-state characteristics shown in Fig. 3. It is apparent that the

electrolyzer has a very narrow voltage range which translates into a very current-sensitive operation range. Moreover, it shows an almost perfect resistive load behavior at steady-state. Accordingly, the requirements of the DC-DC interleaved converter are defined according to the parameters specified in table I.

TABLE I  
PARAMETERS TABLE PER CONVERTER

Parameter	$V_{in}$	$\Delta I_L$	$\Delta V_{out}$	$L$	$C$	$F_{switching}$
Value	150 V	0.3 A	0.1 V	2.5 mH	12.5 $\mu$ F	20 kHz

### B. Single DC-DC buck model

For a single buck converter, starting from the steady state transfer function relating the change in the inductor current ( $\Delta I_L$ ) to duty cycle value ( $\Delta D$ ) introduced in [9]:

$$\begin{aligned}
 H(s) &= \frac{\Delta I_L}{\Delta D} = \frac{V_{in}}{L} * \frac{(s + \frac{1}{RC})}{(s^2 + \frac{1}{RC}s + \frac{1}{LC})} \\
 &= \frac{V_{in}}{L} * \frac{(s + z_1)}{(s + p_1)(s + p_2)}
 \end{aligned} \quad (1)$$

Where  $L$  is the inductor value [H],  $C$  is the output capacitor value [F],  $V_{in}$  is the converters input voltage [V], and  $R$  is the load resistance value [ $\Omega$ ].

This highlights the effect of the load value upon the positions of the poles and zeros of the system, as the roots of the characteristic function are:

$$s_{1,2} = \frac{-L \pm \sqrt{L(L - 4CR^2)}}{2LCR} \quad (2)$$

By observing the open-loop pole-zero map (Fig. 4), when varying the reference current from 7.5 A to 150 A, a huge variation in the locations of the poles and zeros of the system is clear, moving from complex pair to real pair as the power

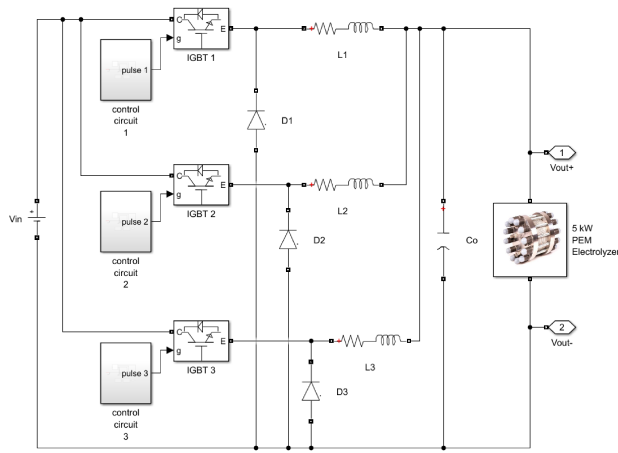


Fig. 2. MATLAB/Simulink model of the system.

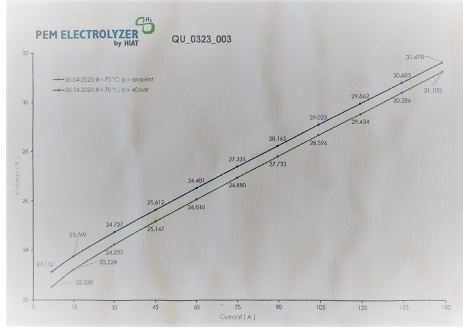


Fig. 3. Polarization curves of the 5 kW PEM electrolyzer.

increases. It is worth noticing though that the system is very fast with a high damping. Accordingly, the controller needs to keep the high damping ratio while the speed part is to be adapted to the electrolyzer's dynamics.

For the demonstration of the controller design process, the maximum point of operation (150 A) is chosen as an example, where the process is then generalized for the whole operation range. Fig. 5 shows the open loop root locus of the system at the 150 A reference current where it is apparent that the main pole shaping the locus is  $(p_2 = \frac{=L+\sqrt{L(L-4CR^2)}}{2LCR})$ .

### C. Lead-lag controller design

1) *Lead compensator*: A lead compensator serves the purpose of shifting the root locus of a system to the left-hand side of the  $j\omega$  axis giving more stability and a faster response to the system [14]. This is achieved by introducing a pole  $p_{lead}$  with a higher magnitude than the zero  $z_{lead}$  in the transfer function (3) representing it.

A gain  $K_{lead}$  is also required to ensure that the closed-loop root locus will pass through the intended poles that satisfy the

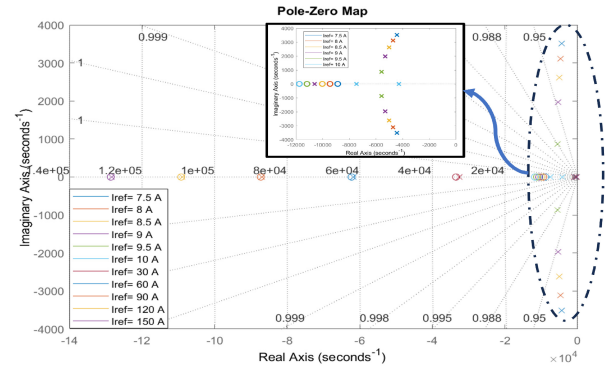


Fig. 4. Open loop pole-zero map of the converter over the operation range.

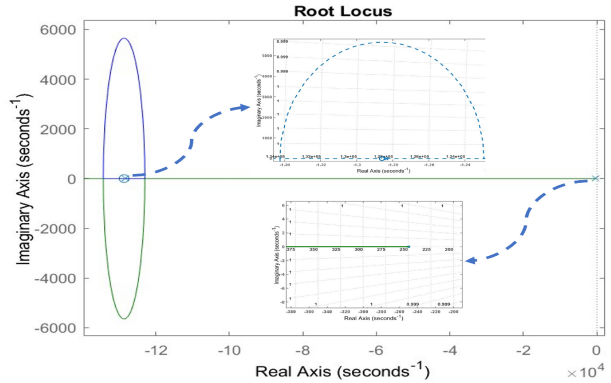


Fig. 5. Open loop root locus of the converter at 150A.

intended response.

$$C(s)_{lead} = K_{lead} * \frac{(s + z_{lead})}{(s + p_{lead})} \quad (3)$$

For the test case, the zero of the lead compensator ( $z_{lead}$ ) is chosen to be placed at the system's dominant pole ( $p_2$ ). Therefore, the behavior of the system will be determined based on the place of the lead compensator pole ( $p_{lead}$ ) location. For a critically damped system, a damping ratio ( $\zeta$ ) of 1 is selected and the pole ( $p_{lead}$ ) is placed at ( $p_c = 5 - 8 * 10^6$ ) on the real axis ( $\sigma\omega$ ). The high value of  $p_{lead}$  is due to the later addition of a lag compensator which will slow down the system for a low steady-state error value.

The overall gain ( $K$ ) needed for the system with the lead compensator is described as the ratio between the product of the lengths of poles ( $L_p$ ) divided by the length of zeros ( $L_z$ ):

$$K = \frac{\prod L_p}{\prod L_z} = \frac{L_{p1} * L_{p2}}{L_{z1} * L_{z_{lead}}} = \frac{L_{p1}}{L_{z1}} \quad (4)$$

As so, it can be generalized along with the open loop gain

from (1) to be:

$$K = K_{lead} * \frac{V_{in}}{L} = \frac{\sqrt{(|(P_c| - |Re(P_1)|)|^2 + |Im(P_1)|)^2}}{|(P_c| - |\frac{1}{RC}|)|} \quad (5)$$

Where  $Re(P_1)$  is the real part of the pole and  $Im(P_1)$  is the imaginary part. Thus, the open loop transfer function with the lead compensator becomes:

$$H_{ol_{lead}} = \frac{V_{in}}{L} * K_{lead} * \frac{(s + z_1)}{(s + p_1)(s + p_c)} \quad (6)$$

2) *Lag compensator*: The lag compensator transfer function is similar to the lead compensator one with the absence of the gain and the fact that the zero magnitude is larger than the pole magnitude. Accordingly, it can be defined as:

$$C(s)_{lag} = \frac{(s + z_{lag})}{(s + p_{lag})} \quad (7)$$

In order to determine if a lag compensator is needed, or in particular, how to design it, the steady-state error ( $E_{ss}$ ) is to be calculated according to:

$$E_{ss} = \lim_{s \rightarrow 0} s * \frac{1}{s * (1 + H_{ol_{lead}})} \quad (8)$$

By substituting (6) in (8), the steady-state error value becomes:

$$E_{ss} = \frac{p_1 * p_c}{(p_1 * p_c) + (K * |z_1|)} \quad (9)$$

It deems necessary from (9) that the system will need a lag compensator as the steady-state error is dependent on the placing of the lead compensator pole, zero, and gain ( $\neq 0$ ). Thus, via imposing a set point of 1% steady-state error and substituting in (9), the ratio between the zero and pole of the lag compensator is to be:

$$\frac{|p_{lag}|}{|z_{lag}|} = \frac{0.99 * (P_c * P_1)}{0.01 * K * |z_1|} \quad (10)$$

#### D. Control circuit implementation

For a real-time digital (dSPACE) implementation of the control block indicated in Fig. 2, the Simulink model of the control block calculates the poles and the zero of the system in real-time based on the value of the resistance of the load per converter (i.e electrolyzer resistance multiplied by the number of interleaved converters) as in Fig. 6. The resistance is defined from the polarization curve of the electrolyzer (Fig. 3) based on the reference current signal. These values along with the selected pole ( $p_c$ ) are used to calculate the "adapted" lead controller gain ( $K_{lead}$ ) for the system which afterward (Fig. 7) is fed to the transfer functions of the lead-lag controller. The controller calculates the duty cycle needed per converter to generate the required pulse-width modulation (PWM) signals. To achieve the required ripple current level at the load side, each converter PWM generator has a phase shift of  $120^\circ$ . For the insurance of load sharing between the interleaved converters, each converter control loop takes as a feedback signal the respective inductor current. Thus, the decoupling of current control is achieved.

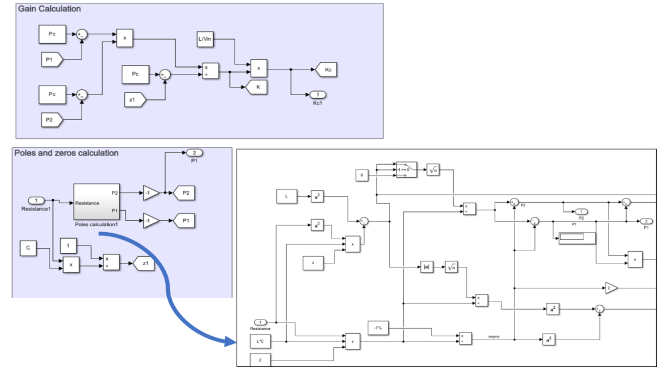


Fig. 6. Poles, zero and controller gain calculation block.

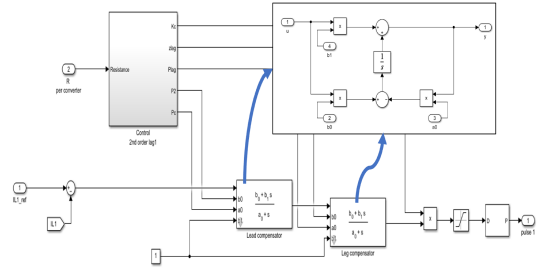


Fig. 7. Lead-lag controllers blocks.

### III. RESULTS AND DISCUSSIONS

The controller parameters were designed to achieve the power requirements defined in table I and a settling time of 50 ms. The first test was a step response from 0% to the rated current of 150A. Fig. 8 views the response of the system. It shows that the controller manages to achieve the requirements defined. The steady-state error is around 0.3%. This percentage proves the correct current sharing within the interleaved converters as it is  $\frac{1\%}{3}$ . The same effect can be observed in the ripple current percentage which is one-third of the value designed per converter.

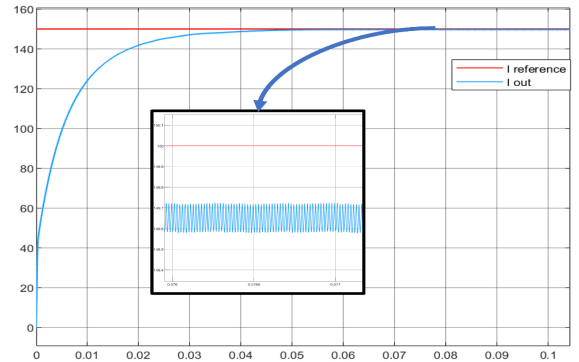


Fig. 8. Step response from 0-100%.

The next step for validating the control scheme was a series of very fast changing up and down ramps. The power set-points changed from 20% to 100% of the rated power of the electrolyzer, which are the ranges within which the electrolyzers normally operate. Fig. 9 shows the response behavior which results in the same ripple current level of 0.1 A and a steady-state error of 0.2% in the mid-range of operation, which follows the design milestones.

Fig. 10 highlights the current sharing between the converters at identical components case (same inductors value). The same test was rerun assuming a mismatch between the inductor's values to assure the stability and robustness of the controller. The inductors values were varied by +20%, +5%, and -10% for converters 1,2, and 3 respectively. These are typical values specified in inductors datasheets. The results are shown in Fig. 11 where it can be seen an almost identical steady-state error value as the balanced case. However, a slight increase in the current ripple can be observed due to the mismatch per converter current, which in turn results in a non-complete cancellation of the ripples. This can be seen more clearly in Fig. 12 which shows the current per inductor and thus the summation of the 3 gives the total current for the load. Nevertheless, the control proves its ability to operate at the reference signals regardless of the mismatch of the components and at different operating points of the electrolyzer.

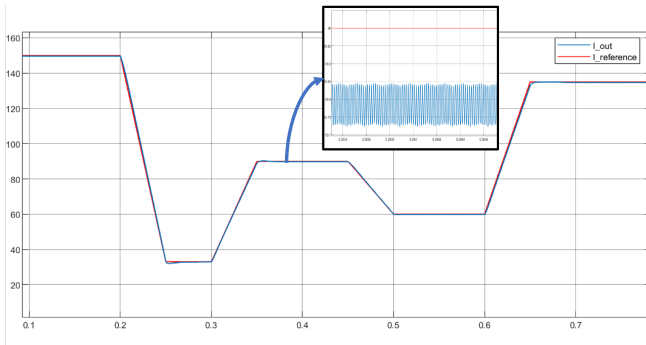


Fig. 9. Ramp response- identical components- ranging from 20-100%.

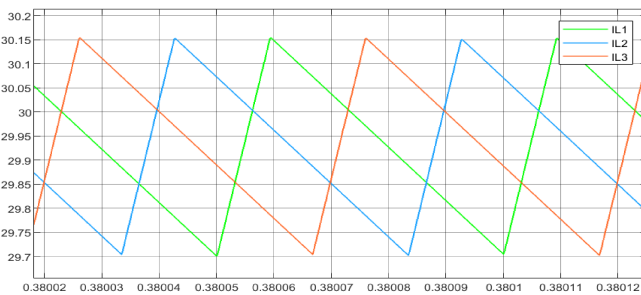


Fig. 10. Current sharing at identical components case.

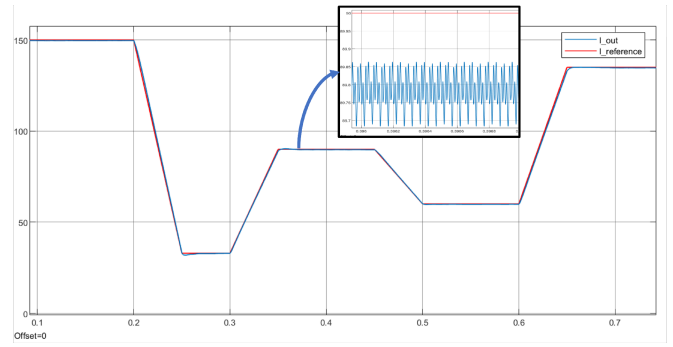


Fig. 11. Ramp response- unbalanced components- ranging from 20-100%.

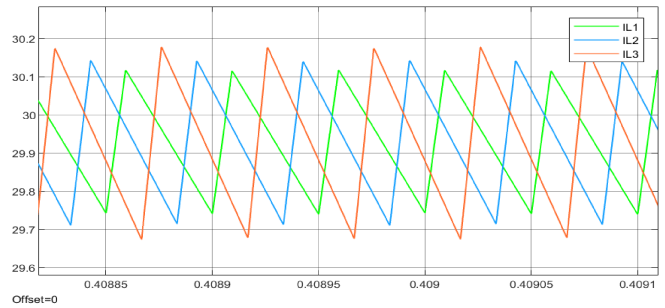


Fig. 12. Current sharing at unbalanced components case.

#### IV. CONCLUSION AND FUTURE WORK

This investigation proposed a new control approach for a current-controlled interleaved buck converter to cover the large operational range while maintaining a very low current ripple level at the stack level of the modular high-power PEM hydrogen electrolyzer. By observing the locations of the poles and zeros of the system on the root locus, the adaptive lead-lag compensator is able to satisfy the control requirements and the current sharing at balanced and unbalanced component values. MATLAB/Simulink validation results were presented for step and ramp responses of the system, resulting in under 1% steady-state error and 0.1 A current ripple at all test cases. This validates the compatibility of the control approach to enable PEM electrolyzer in following grid ancillary services control signals.

The next step for the validation and testing of the control system is via experimental results. A similar system to the one illustrated in Fig.1 would be constructed. All the control signals including the newly proposed controller will be implemented using the dSPACE platform and be connected to the active rectifier (Fig.13), middle bus buck converter, and the interleaved buck converter. The power system will be used along with the currently in-commission 5 kW electrolyzer (Fig. 14). The integrated system of the converters plus the electrolyzer is to be connected to a power amplifier and real-time digital simulator (RTDS) (Fig.15) testing the performance of the control when connected to grid models and faults.



Fig. 13. PQ controlled active rectifier.



Fig. 14. 5kW PEM electrolyzer.

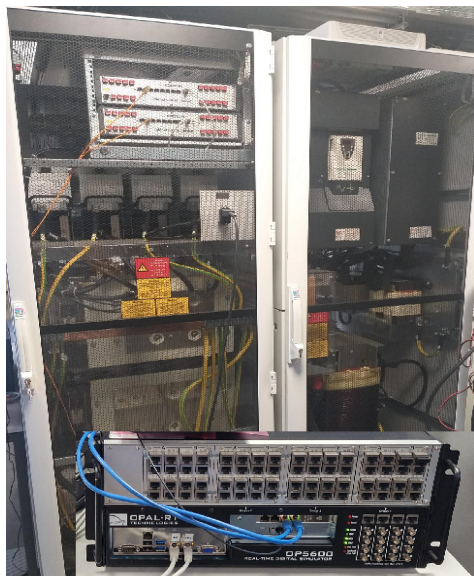


Fig. 15. Power amplifier and RTDS.

## REFERENCES

- [1] REN21, "Renewables 2022 Global Status Report," (Paris: REN21 Secretariat), <https://www.ren21.net/reports/global-status-report/>, 2022, ISBN 978-3-948393-04-5, [Online: accessed 2023/06/20]
- [2] B. L. H. Nguyen, M. Panwar, R. Hovsopian, K. Nagasawa and T. V. Vu, "Power Converter Topologies for Electrolyzer Applications to Enable Electric Grid Services," IECON 2021 – 47th Annual Conference of the IEEE Industrial Electronics Society, Toronto, ON, Canada, 2021, pp. 1-6, doi: 10.1109/IECON48115.2021.9589044.
- [3] Mohamed Keddar, Zhifeng Zhang, Chendhil Periasamy, Mamadou Lamine Doumbia, "Power quality improvement for 20 MW PEM water electrolysis system," International Journal of Hydrogen Energy, Volume 47, Issue 95, 2022, Pages 40184-40195, ISSN 0360-3199, <https://doi.org/10.1016/j.ijhydene.2022.08.073>.
- [4] Henning P.C. Buitendach, Rupert Gouws, Christiaan A. Martinson, Carel Minnaar, Dmitri Bessarabov, "Effect of a ripple current on the efficiency of a PEM electrolyser," Results in Engineering, Volume 10, 2021, 100216, ISSN 2590-1230, <https://doi.org/10.1016/j.rineng.2021.100216>.
- [5] H. Renaudineau, A. M. Llor, R. Cortés D., C. A. Rojas, C. Restrepo and S. Kouro, "Photovoltaic Green Hydrogen Challenges and Opportunities: A Power Electronics Perspective," in IEEE Industrial Electronics Magazine, vol. 16, no. 1, pp. 31-41, March 2022, doi: 10.1109/MIE.2021.3120705.
- [6] E. Escobedo, D. García, M. Ruiz, A. Izquierdo, D. Pacheco-Catalán, L.C. Ordóñez, "Design, construction, and performance of a proton exchange membrane water electrolyzer (PEM-WE)," International Journal of Electrochemical Science, Volume 18, Issue 5, 2023, 100110, ISSN 1452-3981, <https://doi.org/10.1016/j.ijeos.2023.100110>.
- [7] Xinyu Lu, Banghua Du, Shenpei Zhou, Wenchao Zhu, Yang Li, Yang Yang, Changjun Xie, Bo Zhao, Leiqi Zhang, Jie Song, Zhanfeng Deng, "Optimization of power allocation for wind-hydrogen system multi-stack PEM water electrolyzer considering degradation conditions," International Journal of Hydrogen Energy, Volume 48, Issue 15, 2023, Pages 5850-5872, ISSN 0360-3199, <https://doi.org/10.1016/j.ijhydene.2022.11.092>.
- [8] UCTE, "Appendix 1: Load frequency control and performance," 2004, <http://entsoe.eu/cleandocuments/pre2015/publications/entsoe/OperationHandbook/PolicyAppendix%20final.pdf>, [Online: accessed 2023/06/22].
- [9] Y. Zhao, W. Qiao and D. Ha, "A Sliding-Mode Duty-Ratio Controller for DC/DC Buck Converters With Constant Power Loads," in IEEE Transactions on Industry Applications, vol. 50, no. 2, pp. 1448-1458, March-April 2014, doi: 10.1109/TIA.2013.2273751.
- [10] Xiaoqiang Guo, et al., "A new multi-mode fault-tolerant operation control strategy of multiphase stacked interleaved Buck converter for green hydrogen production," International Journal of Hydrogen Energy, Volume 47, Issue 71, 2022, Pages 30359-30370, ISSN 0360-3199, <https://doi.org/10.1016/j.ijhydene.2022.06.249>.
- [11] Damien Guilbert, Dario Sorbera, Gianpaolo Vitale, "A stacked interleaved DC-DC buck converter for proton exchange membrane electrolyzer applications: Design and experimental validation," International Journal of Hydrogen Energy, Volume 45, Issue 1, 2020, Pages 64-79, ISSN 0360-3199, <https://doi.org/10.1016/j.ijhydene.2019.10.238>.
- [12] Yodwong B, Guilbert D, Kaewmanee W, Phattanasak M., "Energy Efficiency Based Control Strategy of a Three-Level Interleaved DC-DC Buck Converter Supplying a Proton Exchange Membrane Electrolyzer," Electronics, 2019, 8(9):933, <https://doi.org/10.3390/electronics8090933>
- [13] M. O. Younsi, M. Bendali, T. Azib, C. Larouci, C. Marchand and G. Coquery, "Current-sharing control technique of interleaved buck converter for automotive application," 7th IET International Conference on Power Electronics, Machines and Drives (PEMD 2014), Manchester, UK, 2014, pp. 1-6, doi: 10.1049/cp.2014.0448.
- [14] Nise, N.S., "Control Systems Engineering," Sixth ed., John Wiley & Sons, Incorporated, 2011, pp. 477-481, ISBN 9781118138168.